Journal of Extracellular Vesicles

co-action PUBLISHING

ORIGINAL RESEARCH ARTICLE

Characterization of procoagulant extracellular vesicles and platelet membrane disintegration in DMSO-cryopreserved platelets

Tseday Z. Tegegn, Silvia H. De Paoli, Martina Orecna, Oumsalama K. Elhelu, Samuel A. Woodle, Ivan D. Tarandovskiy, Mikhail V. Ovanesov and Jan Simak*

Office of Blood Research and Review, Center for Biologics Evaluation and Research, U.S. Food and Drug Administration, Silver Spring, MD, USA

Background: Freezing is promising for extended platelet (PLT) storage for transfusion. 6% DMSO cryopreserved PLTs (CPPs) are currently in clinical development. CPPs contain significant amount of platelet membrane vesicles (PMVs). PLT-membrane changes and PMV release in CPP are poorly understood, and haemostatic effects of CPP PMVs are not fully elucidated. This study aims to investigate PLT-membrane alterations in CPPs and provide comprehensive characterization of CPP PMVs, and their contribution to procoagulant activity (PCA) of CPPs.

Methods: CPPs and corresponding liquid-stored PLTs (LSPs) were characterized by flow cytometry (FC), fluorescence polarization (FP), nanoparticle tracking analysis (NTA), electron microscopy (SEM, TEM), atomic force microscopy (AFM) and thrombin-generation (TG) test.

Results: SEM and TEM revealed disintegration and vesiculation of the PLT-plasma membrane and loss of intracellular organization in 60% PLTs in CPPs. FP demonstrated that 6% DMSO alone and with freezing–thawing caused marked increase in PLT-membrane fluidity. The FC counts of annexin V-binding PMVs and $CD41a^{+}$ PMVs were 68- and 56-folds higher, respectively, in CPPs than in LSPs. The AFM and NTA size distribution of PMVs in CPPs indicated a peak diameter of 100 nm, corresponding to exosome-size vesicles. TG-based PCA of CPPs was 2- and 9-folds higher per PLT and per volume, respectively, compared to LSPs. Differential centrifugation showed that CPP supernatant contributed 26% to CPP TG-PCA, mostly by the exosome-size PMVs and their TG-PCA was phosphatidylserine dependent.

Conclusions: Major portion of CPPs does not show activation phenotype but exhibits grape-like membrane disintegration with significant increase of membrane fluidity induced by 6% DMSO alone and further aggravated by freezing–thawing process. DMSO cryopreservation of PLTs is associated with the release of PMVs and marked increase of TG-PCA, as compared to LSPs. Exosome-size PMVs have significant contribution to PCA of CPPs.

Keywords: *extracellular vesicles*; *microparticles*; *platelet physiology*; *blood products*; *thrombin*; *transfusion medicine*; *nanoparticle tracking analysis*; *flow cytometry*; *atomic force microscopy*; *electron microscopy*

Responsible Editor: Raymond M. Schiffelers, University Medical Center Utrecht, Netherlands.

*Correspondence to: Jan Simak, Laboratory of Cellular Hematology, DHRR/OBRR, Center for Biologics Evaluation and Research, Food and Drug Administration, 10903 New Hampshire Avenue, WO Bldg. 52/72, Rm. 4210, Silver Spring, MD 20993-0002, USA, Email: jan.simak@fda.hhs.gov

To access the supplementary material to this article, please see Supplementary files under 'Article Tools'.

Received: 19 November 2015; Revised: 18 March 2016; Accepted: 23 March 2016; Published: 4 May 2016

Blood platelets (PLTs) for transfusion can be stored for only 5–7 days at room temperature (RT). Longer storage is not feasible due to potential bacterial contamination, and the loss of PLT function characterized as storage lesions. Extension of PLT storage time is critical for PLT availability in remote locations, bridging inventory shortages of liquid stored PLT in hospital practice and building a phenotyped and/or genotyped PLT inventory to treat refractory patients (1). PLT freezing would enable long-term storage of this

essential blood component for transfusion medicine (1). The current state-of-the-art method for the preparation of cryopreserved platelets (CPPs), introduced by Valeri and colleagues, is freezing of hyperconcentrated PLTs in 6% dimethyl sulfoxide (DMSO) (2,3). Removal of the PLT supernatant before freezing enables freezing at low volumes and eliminates the need for post-thaw washing (4,5). DMSO is a cell membrane-penetrating cryoprotectant that protects cells from frost injury caused by the intracellular formation of ice during freezing and thawing. DMSO is an amphipathic molecule with a highly polar domain and 2 apolar groups and is therefore soluble in both aqueous and organic media (6). DMSO is widely used for cell and tissue cryopreservation but exhibits various pharmacological activities (6,7), including moderate toxicity (8) that affects the differentiation of different types of cells (9,10). Adverse reactions associated with infusion of DMSO-cryopreserved cells have been documented (11). In contrast to other commonly cryopreserved eukaryotic cells (i.e. stem cells and sperm cells), blood PLTs undergo major functional changes and damage when frozen and thawed in DMSO. An activation phenotype, lower in vivo recovery and decreased in vitro function are the main reported features of DMSO-CPPs (12–14).

Preserving the reactivity and desired functions of PLTs remains a challenge in the development of PLT cryopreservation techniques. Nevertheless, DMSO-CPPs prepared by a variety of protocols have been used clinically for nearly 60 years (15,16). The most extensive experience has been the clinical use of autologous CPPs in the transfusion of alloimmunized thrombocytopenic chemotherapy patients (17). The military use of CPP products is another area of large-scale utility of these products (18,19). In general, the clinical use of CPPs has been documented in anecdotal reports with an absence of controlled randomized trials, except a small study in cardiopulmonary bypass patients that demonstrated a decrease in blood loss and RBC transfusion requirements in CPP-treated patients compared to the liquid-stored PLTs (LSPs) group (14). This result suggests that CPPs are more haemostatically active in vivo than LSPs. Previous in vitro studies indicate that increased haemostatic activity in vivo is due to a procoagulant phenotype of CPPs manifested by plasma membrane exposure of phosphatidylserine (PS) and formation of PS-expressing platelet membrane vesicles (PMVs) (20). PLT-membrane changes in CPP are poorly understood, and haemostatic effects of CPP PMVs are not fully elucidated.

In clinical development of CPP products, comprehensive analysis of CPP PMVs and their procoagulant activity (PCA) are essential for characterization, quality control and establishment of in vitro potency assays which would be relevant to their in vivo haemostatic effects.

Here, we focused on the characterization of PMVs released from CPPs, including exosome-size vesicles with a hydrodynamic diameter of less than 200 nm, a size distribution that is below the limit of detection of conventional flow cytometry (FC). We used high resolution techniques for the analysis of nanoparticles, including atomic force microscopy (AFM) and nanoparticle tracking analysis (NTA), which permitted the characterization of membrane vesicles as small as 30 nm in hydrodynamic diameter. To complement the analytical methods, we developed a modified version of the fluorogenic thrombin generation (TG) test (21) to quantify PCA of PLTs and PMVs in normal pooled plasma. Although the in vitro and in vivo phenotypic functional characteristics of CPPs indicate that the freezing–thawing process leads to activation of PLTs, we demonstrate here that CPPs exhibit dramatic changes in membrane integrity due to the membrane transition process. These membrane changes lead to exposure of PS causing the increase of platelet thrombin generation (TG) activity. In association with plasma membrane vesiculation, CPPs show marked release of PMVs, including large amounts of exosome-size PMVs which are responsible for a significant portion of the PCA of CPP supernatants.

Materials and methods

Apheresis PLT collection and CPP preparation

Apheresis PLTs from normal donors collected using an MCS + LN 9000 (Haemonetics, Braintree, MA) in 1:10 of acid citrate dextrose (ACD) to blood ratio were obtained from the Department of Transfusion Medicine, National Institute of Health (Bethesda, MD). Consecutive units collected for research purpose were used; individual donor characteristics such as sex and age were not followed in this study. CPPs were prepared within 24 h after collection according to Valeri's 6% DMSO no-wash protocol (4,5). For our study, CPPs were prepared in aliquots (Supplementary Fig. 1A), with final freezing volume of 2 mL in $-80^{\circ}C \pm 15^{\circ}C$ for 1 h. Sample was thawed at 37°C, resuspended with 2×2 mL saline (Sigma-Aldrich, St. Louis, MO) and used for analysis. The concentrated CPP when frozen contained 78% plasma (ACD), 16% saline and 6% DMSO. The final thawed and resuspended CPP for analysis were composed of platelets in 26% plasma (ACD), 72% saline and 2% DMSO. LSP samples were composed of platelets in 100% plasma (ACD).

PMV fractionation by differential centrifugation

Aliquots of LSPs and CPPs in eppendorf tubes were centrifuged at 2,600 g for 15 min at 20°C, and supernatants (LSP2K, CPP2K) were collected (Supplementary Fig. 1B). 2K supernatants were centrifuged again at 20,000 g for 15 min at 10°C, and 20K supernatants (LSP20K, CPP20K) were collected. Finally, 20K supernatants were

Citation: Journal of Extracellular Vesicles 2016, **5**: 30422 - http://dx.doi.org/10.3402/jev.v5.30422

ultracentrifuged at 100,000 g for 1 h at 4°C, and 100K supernatants were collected (LSP100K, CPP100K). In addition to all supernatants, 20,000 g and 100,000 g sediments (CPP20Kp, CPP100Kp) were also analysed. In some experiments, LSP processing control (LSP-PC) without DMSO and freezing–thawing step was also spun at 2,600 g (LSP-PC2K) and analysed in parallel to CPP2K PMVs.

Thrombin generation-based procoagulant activity

The in-house developed TG test was performed as described previously (21) with modifications. Briefly, a mixture of freshly thawed normal plasma (Affinity Biologicals Inc., Ontario, Canada), 1 × Tris-BSA buffer, pH 7.3 (Aniara Diagnostica LLC, West Chester, OH) and tissue factor (Dade Innovin, Marburg, Germany) was prepared. In a round-bottom 96-well sample preparation plate, serial dilutions of PLT and PMV samples were prepared at 2- or 4-folds in 1 × Tris-BSA buffer. The highest concentration in the reaction plate was on average 480,000 PLT/μL for LSPs and 800,000 PLT/μL for CPPs. Samples were transferred from the round-bottom preparation plate to a 96-well half-area plate in symmetrically positioned duplicates. Then, Z-Gly-Gly-Arg-AMC. HCl substrate (Bachem, Bubendorf, Switzerland) and $CaCl_2$ (Sigma-Aldrich) were added to the plasma mixture. Immediately before recording fluorescence, the recalcified plasma mixture was transferred from a single-well basin to samples in a half-area plate using a 96-channel Matrix Hydra II liquid handling system (Thermo Scientific, Hudson, NH). The wells in the reaction plate comprised PLT and PMV samples (35% vol/vol), normal plasma (50% vol/vol), tissue factor (0.2 pmol/L), Tris-BSA buffer (11.15% vol/vol), fluorogenic substrate (1.25% vol/vol, 800 μmol/L) and $CaCl_2$ (2.4% vol/vol, 12 mmol/L). The fluorescence kinetics was measured at an excitation of 360/40 nm and emission at 460/40 nm in a Synergy H4 (Biotek, Winooski, VT) at 37°C. UPTT standardized rabbit brain phospholipids (Bio/Data Corporation, Horsham, PA) and CPP control (200,000 PLT/μL; prepared in multiple aliquots from a single donor and stored at −80°C) were used as assay controls. The data were processed using a software package designed by Dr. Mikhail Ovanesov using OriginPro (OriginLab, Northampton, MA), described previously (22). Raw fluorescence was converted into thrombin activity units using an internal thrombin calibrator from Stago USA (Parsippany, NJ). Thrombin peak height (TPH) (nmol/L) was selected as the best representative parameter of thrombin-generating PCA (TG-PCA). The TG-PCA results for CPPs and LSPs were calculated per 1 PLT in the reaction well and per 1 μL of corresponding units. Raw fluorescence was converted into thrombin activity units using an internal thrombin calibrator (Stago USA). TPH parameter was analysed to obtain TG-PCA of LSPs and CPPs per 1 PLT and per 1 μL of corresponding units. The following parameters were also evaluated: the lag time (min), that is, the time to reach 17% of TPH; the time to peak (min); and the endogenous thrombin potential (ETP; nmol/L x min), which represents the area under the TG curve. Experiments to inhibiting TG by blocking PS was performed by incubating 100 μL aliquot of undiluted CPP20K with 5, 10 and 30 μg/mL lactadherin (Haematologic Technologies Essex Junction, VT) or with annexin V (BD Biosciences, San Diego, CA). As a control for annexin V inhibitory activity, annexin V was pre-incubated with anti-annexin V rabbit polyclonal antibody (BioVision, Inc., Milpitas, CA).

Flow cytometric analysis of PLTs and PMVs

To assess PLT surface antigens and activation markers (23), LSPs and CPPs were diluted in Tyrode's salt solution (TSS) (Sigma-Aldrich) to 30,000 PLTs/μL. 50 μL of CPPs and LSPs were incubated for 20 min at RT in the dark with saturating concentrations of monoclonal antibodies against CD41a (FITC), CD62P (PE) and annexin V (PE) with 2 mM Ca^{2+} binding buffer (BD Biosciences, San Diego, CA). Then, samples were washed with TSS at 2,000 g for 10 min in RT, resuspended in 500 of TSS right before analysis and immediately analysed using an LSRII flow cytometer (BD Biosciences) with forward scatter (FSC) and side scatter (SSC) in logarithmic mode. Non-labelled and isotype control-labelled samples were analysed in parallel.

For PMV analysis (24), CPP2K were diluted with HBSS/Ca^{2+}/BSA, to get 1,000 events per second during analysis. 50 μL of LSP2K and CPP2K samples was stained with CD41a (PE) and annexin V (FITC) (BD Biosciences) or lactadherin (FITC) (Haematologic Technologies). Matching isotype controls and non-labelled samples were used as controls. After staining, samples were diluted with 450 μL of HBSS/Ca^{2+}/BSA and analysed on FSC channel with PMT. Trucount beads (BD Biosciences) were used for evaluation of sample flow rate (25). NIST Traceable Size Standard polystyrene beads (Bangs Laboratories, Fishers, IN), 200–1,000 nm of hydrodynamic diameter, were used for FSC calibration. Counts of specific phenotypes in PMVs/μL were calculated for original LSP and CPP product. All FC experiments were performed using the LSRII flow cytometer (BD Biosciences) with forward scatter (FSC) and side scatter (SSC) in logarithmic mode. Data were evaluated using FlowJo (Treestar, Ashland, OR).

Light transmission aggregometry

LSPs and CPPs were diluted to 250,000 PLT/μL with corresponding PLT-poor plasma (PPP). Samples were treated with thrombin receptor-activating peptide 6 (TRAP-6) (20 μmol/L) from AnaSpec (Fremont, CA), collagen (5 μg/mL) or adenosine diphosphate (ADP) (20 μmol/L) (Chrono-Log Corp., Havertown, PA). The change in light transmission was recorded for

20 min using Chrono-log 700 (Chrono-Log Corp.). The maximum aggregation response was expressed as the maximum percentage change in light transmittance from baseline (26).

Nanoparticle tracking analysis

PMVs in 2,600 g spun PLT supernatants CPP2K and LSP-PC2K were quantified by NTA using the NanoSight LM10 system from Malvern (Worcestershire, UK), 405 nm LASER, NTA 2.3 software. PMV concentration was adjusted with Tyrode's buffer to achieve 50 to 70 PMVs in the field of view. PMV Brownian motion data were recorded for 90 sec at 22°C at least 3 times; PMVs were introduced into the system manually. The PMV size distribution and count per mL were evaluated using automatic detection threshold, 3×3 blur and minimum track length of 12.

Laser scanning confocal microscopy

The LSPs and CPPs were fixed with 2% paraformaldehyde (PFA) for 20 min, washed with TSS and incubated with 0.1 µmol/L Texas Red® DHPE (Life Technologies, Grand Island, NY) for 30 min at RT. Samples were cytospun onto poly-L-lysine-coated glass slide, washed with PBS, mounted with ProLong Gold Antifade (Life Technologies) and imaged using LSM 700 (Carl Zeiss, Oberkochen, Germany) with 63x/1.40 oil objective (27).

Field emission scanning electron microscopy

LSPs and CPPs were fixed in 4% PFA for 30 min, cytospun onto glass slide, washed with PBS, fixed with 2% glutaraldehyde (GTA) for 1 h, washed extensively with 0.1 mol/L sodium cacodylate buffer (Electron Microscopy Sciences, Hatfield, PA), dehydrated in ethanol series and dried at RT, sputter coated using a high-resolution sputter coater (Ted Pella, Inc., Redding, CA) with a thin film of gold at 13.3 Pa and 45 mA for 90 s. The images were collected with Hitachi S4700 microscope (28). To estimate damaged PLTs in CPPs, 7 large-field images were collected, and percentages of damaged PLTs with rough, porous membranes and grape-like structures were counted.

Transmission electron microscopy

LSPs, CPPs, CPP20Kp and CPP100Kp were fixed in 4% PFA and 1% GTA for 1 h and post-fixed in 1% osmium tetroxide (OsO_4) solution in 0.1 mol/L sodium cacodylate buffer. Samples were then dehydrated in ethanol series, embedded with EMBed-812 and polymerized for 3 days at 65°C. Approximately 50 nm sections were cut on Leica EM UC7 (Leica Microsystems, Buffalo Grove, IL), collected onto 600-mesh copper grids and imaged with JEOL 1400 microscope operating at 80 kV accelerating voltage (29).

Atomic force microscopy

CPP2K and CPP100Kp were fixed in 0.5% GTA and 2% PFA for 5 min and adsorbed onto a freshly cut mica pre-coated with 1% poly-L-lysine for 10 min, washed with PBS. Samples in PBS were imaged with Cypher AFM (Asylum Research, Santa Barbara, CA) in AC mode using BioLever Mini cantilever (Olympus, Center Valley, PA) with high resonance $\sim$25 kHz in water and spring constant $\sim$0.1 N/m.

Fluorescence polarization

PLTs isolated from LSPs (iPLTs) by 1,230 g centrifugation for 25 min were resuspended to 200,000 iPLTs/µL with saline and incubated with 1 µM 1,6-diphenyl-1,3,5-hexatriene (DPH; Sigma-Aldrich) for 30 min (30). The 360/420 nm fluorescence of DPH was measured for iPLTs incubated at RT without DMSO (LSPs), at RT with 6% DMSO (6% DMSO LSPs), frozen/thawed with 6% DMSO (CPPs) and positive control treated with 30 nmol/L membrane fluidizer halothane (Sigma-Aldrich) (31). Polarization (P) was calculated according to the formula $P = (I_{II} - I_{\perp})/(I_{II} + I_{\perp})$, where I_{II} and $I_{\perp}$ are the intensities of fluorescence when the emission and excitation polarizers are parallel (I_{II}) or perpendicular ($I_{\perp}$) to each other (30). The result is presented as the decrease in polarization ($-\triangle$ DPH polarization, %).

Statistical analysis

If not specified otherwise, the results were calculated from at least 3 independent experiments. The data are presented as means $\pm$ SD. Significant differences were determined using the Wilcoxon signed-rank test, Mann–Whitney and t-test, as appropriate. The data were plotted and analysed using GraphPad Prism 5.0 Software, GraphPad Software, Inc. (San Diego, CA).

Results

Field emission scanning electron microscopy (FESEM) analysis revealed marked disintegration and vesiculation of the plasma membrane in approximately 60% of the PLT population in CPPs (Fig. 1a). These include grape-like changes in about 40% CPPs lacking any pseudopodia formation. These changes indicate loss of plasma membrane integrity rather than activation. Rest of CPPs showed activation phenotype with limited pseudopodia formation. In contrast, the near resting or slight activation phenotype was observed in the majority of the LSPs (Fig. 1a). Transmission electron microscopy (TEM) analysis confirmed the FESEM findings. In contrast to LSPs, CPPs exhibited marked disintegration of PLT infrastructure with peripheral organization of granules. In addition, the loss of reactivity to strong PLT agonist was observed in CPPs. While LSPs showed typical activation response to TRAP-6 (20 µmol/L), CPPs exhibited a lack of change in shape and pseudopodia

Citation: Journal of Extracellular Vesicles 2016, 5: 30422 - http://dx.doi.org/10.3402/jev.v5.30422

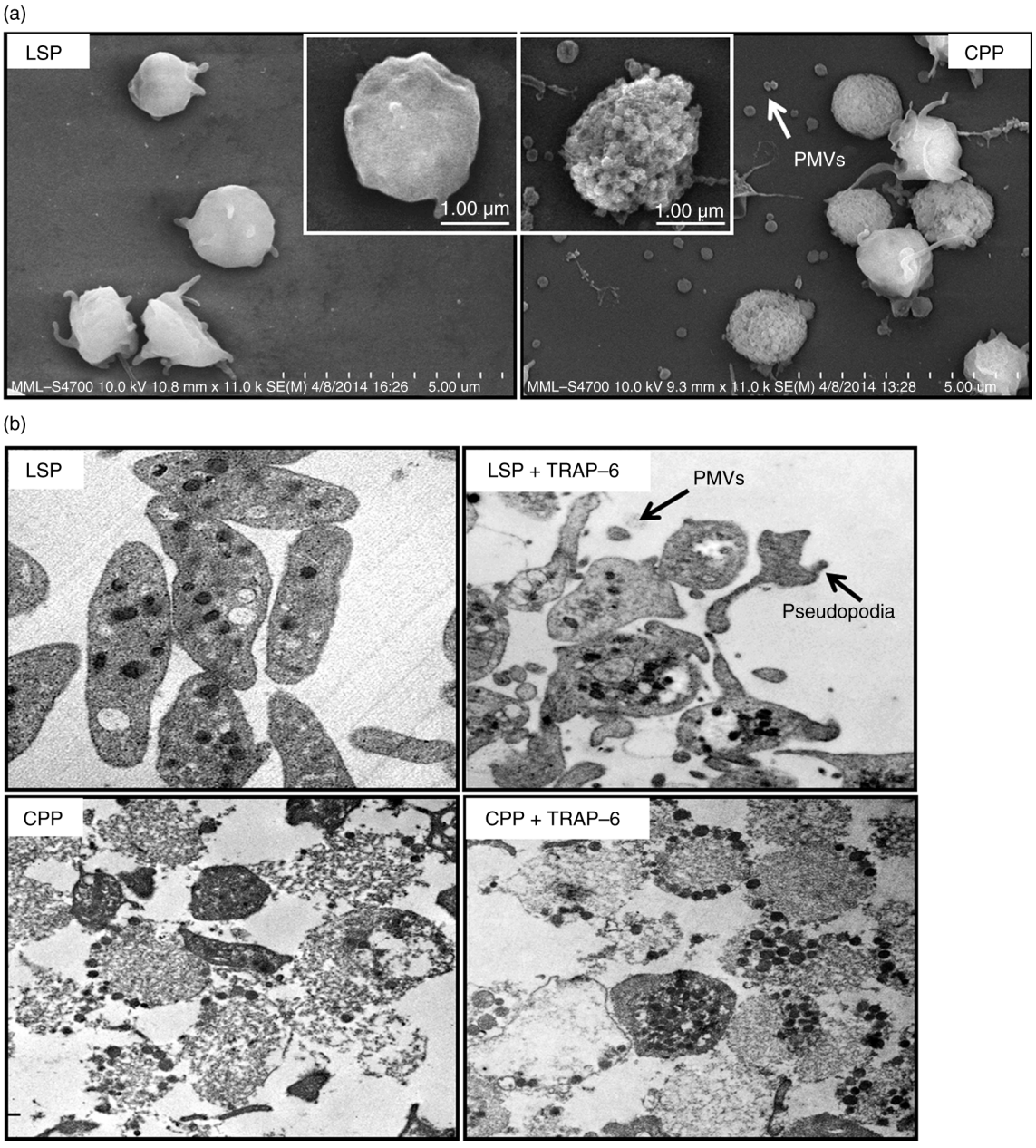

Fig. 1. CPPs exhibited distinct membrane changes by field emission scanning electron microscopy (FESEM) analysis, disturbance of intracellular organization and lack of activation response observed by transmission electron microscopy (TEM). (a) FESEM analysis of liquid-stored platelets (LSPs) and cryopreserved platelets (CPPs). (b) TEM of resting and thrombin receptor activating peptide (TRAP-6, 20 µM) activated liquid-stored PLTs (LSPs) and cryopreserved PLTs (CPPs).

formation (Fig. 1b). In accord with TEM analysis, light transmission aggregometry (LTA) revealed a normal response of LSPs to different activation agonists, including TRAP-6, collagen or ADP. By contrast, CPPs exhibited no aggregation response to collagen and ADP, and a weak reversible aggregation response to the strongest agonist, TRAP-6 (20 µmol/L) (Supplementary Fig. 2).

Laser scanning confocal microscopy (LSCM) revealed high counts of PMVs in CPPs (Supplementary Fig. 3). TEM analysis of 20,000 g sediment (CPP20Kp) showed high concentration of PMVs with a diameter of 20–500 nm; subpopulations of small exosome-size PMVs 20–150 nm could be further sedimented at 100,000 g (CPP100Kp) from 20,000 g supernatant (CPP20K) (Fig. 2a). To exclude a possibility of artifactual formation of small PMVs during sample processing, the results were confirmed by AFM analysis of 2,600 g supernatant (CPP2K) and exosome-size PMVs or 100,000 g sediment (CPP100Kp) (Fig. 2b).

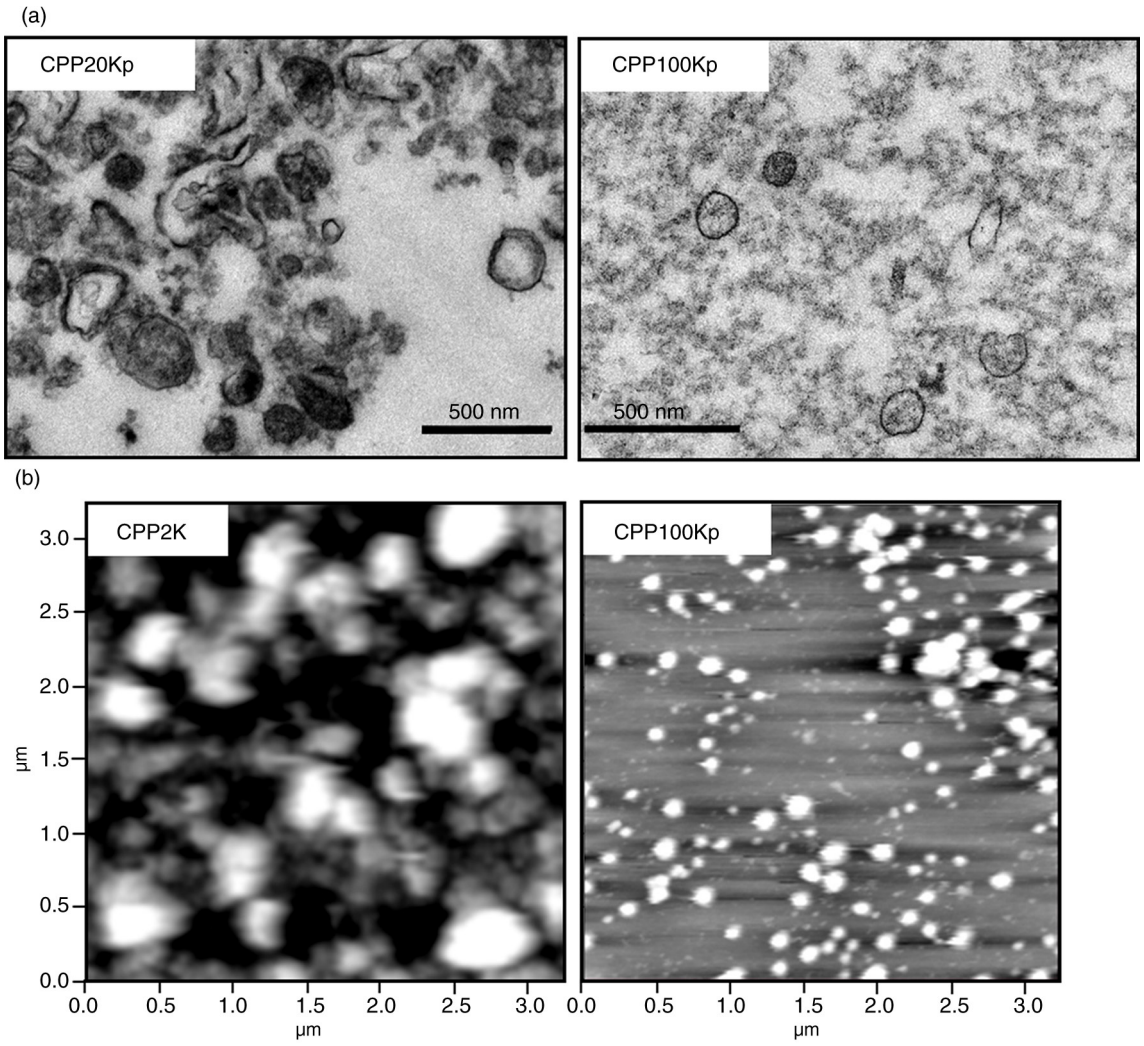

Fig. 2. Transmission electron microscopy (TEM) and atomic force microscopy (AFM) analysis of platelet membrane vesicles (PMVs) in cryopreserved PLTs (CPPs). (a) Transmission electron microscopy (TEM) of PMVs in pellet of 20,000 g spun CPP2K (CPP20Kp) and 100,000 g spun CPP20K (CPP100Kp). (b) AFM analysis of PMVs in supernatant of 2,600 g spun CPP (CPP2K) and pellet of 100,000 g spun CPP20K (CPP100Kp).

We further investigated whether the observed membrane disintegration of CPPs is associated with changes in platelet phospholipid membrane fluidity (32,33). DPH fluorescence polarization (FP) assays demonstrated that treatment of LSPs with 6% DMSO without a freezing–thawing step caused a significant increase in membrane fluidity. Moreover, after the freezing–thawing step, CPPs exhibited a marked increase in membrane fluidity equivalent to the positive control, halothane-treated LSPs (Fig. 3).

FC demonstrated that $69 \pm 12\%$ of PLTs in CPPs had exposed PS in contrast to $11 \pm 10\%$ in LSPs, as detected by annexin V binding (Fig. 4). CPPs also showed marked increase in surface expression of CD62P ($61 \pm 15\%$) compared to LSPs ($18 \pm 6\%$) (Fig. 4). In addition, CPPs contained approximately 68-folds more FC-detectable annexin V-binding PMVs and 56-folds FC-detectable $CD41^+$PMVs more per volume compared to LSPs (Fig. 5a, b). The FSC histogram of CPP PMVs revealed a peak corresponding to 200 nm polystyrene beads and was similar to that of the LSP PMVs (Fig. 5c). As size distribution of exosome-size PMVs is below the limit of reliable detection of FC, we used NTA to compare PMV counts and size distribution in CPP2K reaching the size resolution limit as low as 30 nm of particle hydrodynamic diameter. NTA indicated a 5-fold higher count of exosome-size PMVs in CPP2K compared to LSP-PC2K. 2K supernatant from LSP-PC was used for NTA to avoid the high background created by plasma protein present in LSP. The peak hydrodynamic diameter of exosome-size PMVs was approximately 120 nm (Fig. 6).

Citation: Journal of Extracellular Vesicles 2016, **5**: 30422 - http://dx.doi.org/10.3402/jev.v5.30422

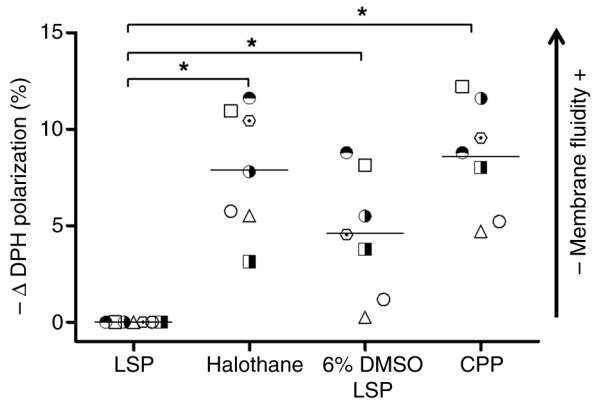

Fig. 3. 6% dimethyl sulfoxide (DMSO) treatment alone and with freezing–thawing increased platelet membrane fluidity. The decrease of DPH fluorescence polarization ($-\delta$ DPH polarization (%)) of liquid-stored platelets (LSPs), LSP with 6% DMSO content without freezing (6% DMSO LSPs) and cryopreserved platelets (CPPs) were assayed. 30 nmol/L membrane fluidizer halothane was used as a positive control. Individual data points normalized with corresponding LSPs are presented in scatter plot (mean); n = 7 donors; *p $\leq$ 0.05.

Both CPPs and LSPs showed a dose response in TG-PCA in plasma in the presence of 0.2 pM tissue factor (Fig. 7a). CPPs exhibited 2-fold higher TG-PCA expressed as TPH per PLT (Fig. 7b). With regard to TG-PCA per volume of resuspended CPP product for infusion, CPPs generated a 9-fold higher TPH/μL compared to LSPs (Fig. 7c). CPPs showed marked differences in other TG test parameters, such as increase in ETP, short TTP and lag time, compared to LSPs (Supplementary Table 1). Differential centrifugation experiments demonstrated that the CPP supernatant (CPP2K) contributed 26.17 $\pm$ 5.6% TG-PCA to CPP (Fig. 8a). The exosome-size PMVs were responsible for most of the CPP2K TG-PCA because the activity remained in the 20,000 g supernatant (CPP20K 24.29 $\pm$ 3.9%) but was substantially decreased in the 100,000 g supernatant (CPP100K 2.85 $\pm$ 1.5%). In addition, TG-PCA could be partially recovered in the 100,000 g pellet (CPP100Kp 10.2 $\pm$ 1.3%) (Fig. 8a). Although LSP exhibited low TG-PCA, the LSP fractions containing PMVs contributed substantial portion of the LSP TG-PCA (LSP2K 82.6 $\pm$ 8.3%; LSP20K 64 $\pm$ 14.4%). This is in agreement with our FC data on annexin V-binding LSP, indicating that whole PLTs in LSP are mostly in resting state and do not contribute to TG-PCA (Fig. 4a, b).

Regarding the mechanism of TG-PCA of CPP PMVs, a dose–response inhibitory effect of lactadherin (Fig. 8b) and inhibition/recovery effects of annexin V/anti-annexin V antibody (Supplementary Fig. 4) on the TG-PCA of the CPP20K supernatant were observed, demonstrating the essential role of exposed PS in TG-PCA of exosome-size PMVs.

In summary, our results showed that the major portion of CPPs does not show activation phenotype but exhibits grape-like membrane disintegration with significant increase of membrane fluidity. PLT membrane disintegration is induced by 6% DMSO alone and further aggravated by freezing-thawing process. DMSO cryopreservation of PLTs is associated with the release of PMVs and marked increase of TG-PCA, as compared to LSPs. Exosome-size PMVs show significant contribution to PCA of CPPs.

Discussion

Early reports of DMSO cryopreservation of PLTs describe abnormalities in PLT aggregation, release reactions, nucleotide content, oxygen consumption, ultrastructural alteration, impairment of phagocytosis, decreased serotonin uptake and decreased response to hypotonic stress (34–36). Significant decreases in intracellular nucleotide content and diminished release of nucleotides following thrombin challenge by CPP, PLT factor 4 activity and decreased oxygen consumption, and PLT aggregation by ADP, epinephrine and collagen have been observed (35,37,38). In a modified Baumgartner chamber, CPPs exhibited a significant decrease in PLT adhesion compared to fresh PLTs and LSPs (39). Morphological damage to DMSO PLTs has also been documented (40); however, a direct link to loss of membrane anisotropy caused by 6% DMSO, as observed in our study, has not been suggested. The morphological and functional disturbances and increased PCA induced by DMSO cryopreservation suggest that DMSO-CPPs are likely to have different safety/efficacy profile than LSPs and may activate coagulation in vivo; thus, DMSO-CPPs should only be used when LSPs are not available (41). Although not an optimal cryoprotectant, DMSO has been well established in PLT cryopreservation in clinical use (16). The optimum DMSO concentration and freezing rate was established based on an in vivo recovery/survival radiolabelling study (42). The DMSO treatment of PLTs without a freezing–thawing step resulted in progressive damage with increasing DMSO concentration (0–15%), as reflected by lower in vivo PLT recovery. This damage was confirmed by our observation of a significant increase of PLT membrane fluidity with 6% DMSO treatment of LSPs without any changes in temperature. Maximum in vivo recovery after the freezing–thawing step was achieved with 5% DMSO-CPPs. As the DMSO concentration increased, the theoretical increase in cryoprotective effect was apparently offset by the DMSO disintegrating effect on PLT membrane and other toxic effects. The freezing rate has been discussed and investigated extensively (43). 5% DMSO-CPPs exhibited the highest in vivo recovery when the freezing rate was 3°C/min, with no significant difference within the range of 1–3°C/min. At freezing rates of 5°C/min and faster,

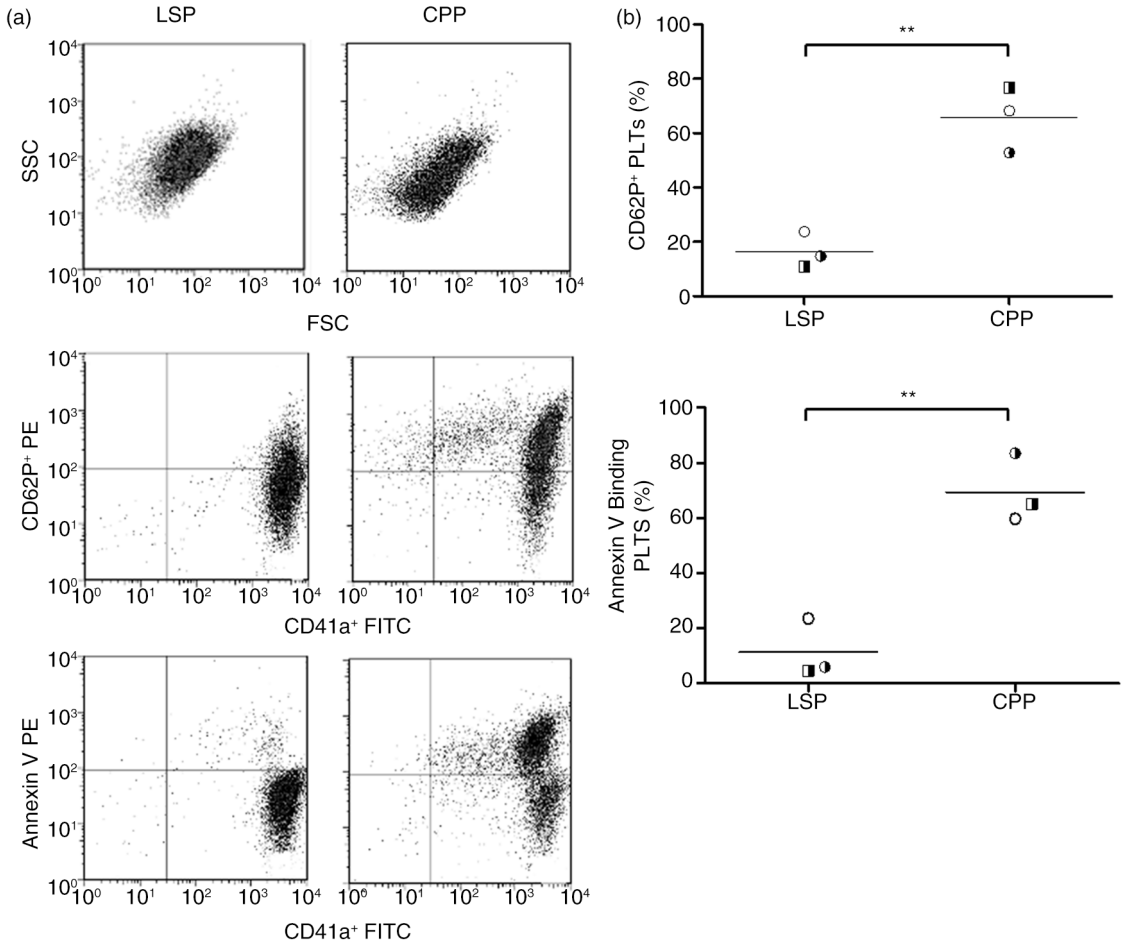

Fig. 4. Flow cytometric analysis showed increase of platelet surface exposure of phosphatidylserine and CD62P on cryopreserved PLTs (CPPs) compared to liquid-stored PLTs (LSPs). (a) LSPs and CPPs representative dot plots showing forward scatter (FSC)/side scatter (SSC), double fluorescence dot plots showing CD41a$^+$ (FITC)/CD62P$^+$ (PE) and CD41a$^+$ (FITC)/annexin V (PE). (b) CD62P$^+$ and annexin V-binding populations in liquid-stored platelets (LSPs) and cryopreserved platelets (CPPs) are calculated as percentage of CD41a$^+$ platelets. Individual data points are shown in scatter plots (mean); n = 3 donors; **$p < 0.01$.

progressively lower in vivo recovery of CPPs was observed, indicating increased PLT damage (42). In our study, the freezing rate 1.8 ± 0.1°C/min was maintained within the optimal range in small aliquots as well as whole CPP units.

We focused our investigation specifically on membrane changes associated with DMSO cryopreservation and characterization of released membrane microvesicles. Although the size distribution of FC detectable PMVs showed a peak FSC value corresponding to 200 nm polystyrene beads, it is important to note that the refractive index of polystyrene (1.605) is higher than membrane vesicles (1.36–1.45), and therefore, the actual size distribution of PMVs detected by FC would be shifted to larger diameters (44). This is in accord with our TEM and AFM analyses showing subpopulations of large PMVs of 200–500 nm in diameter (CPP2K, CPP20Kp). To confirm the TEM results for the size distribution of PMVs and to visualize PMVs in the native state, we used liquid-phase AFM. To separate the different fractions of PMVs, we used a simple differential centrifugation method. Our results revealed that CPPs contained high counts of small exosome-size PMVs of 20–200 nm in diameter (CPP100Kp). The majority of these PMVs are likely the result of transition and disintegration of PLT membranes by DMSO and the freeze–thaw treatment. The potential contribution of naturally occurring PLT exosomes derived from multivesicular bodies, such as organelles, to CPP PMV fractions remains to be investigated. Because conventional FC has very limited detection and size distribution capabilities for phospholipid microvesicles under 200 nm in diameter, we complemented high-resolution FSC-PMT equipped flow cytometry with NTA (44). Based on laser tracking of the Brownian motion of individual vesicles, NTA can evaluate the absolute values of particle hydrodynamic diameter and provide size distribution and counts of membrane vesicles within a size range of 30 nm to approximately 600 nm, thus

Citation: Journal of Extracellular Vesicles 2016, **5**: 30422 - http://dx.doi.org/10.3402/jev.v5.30422

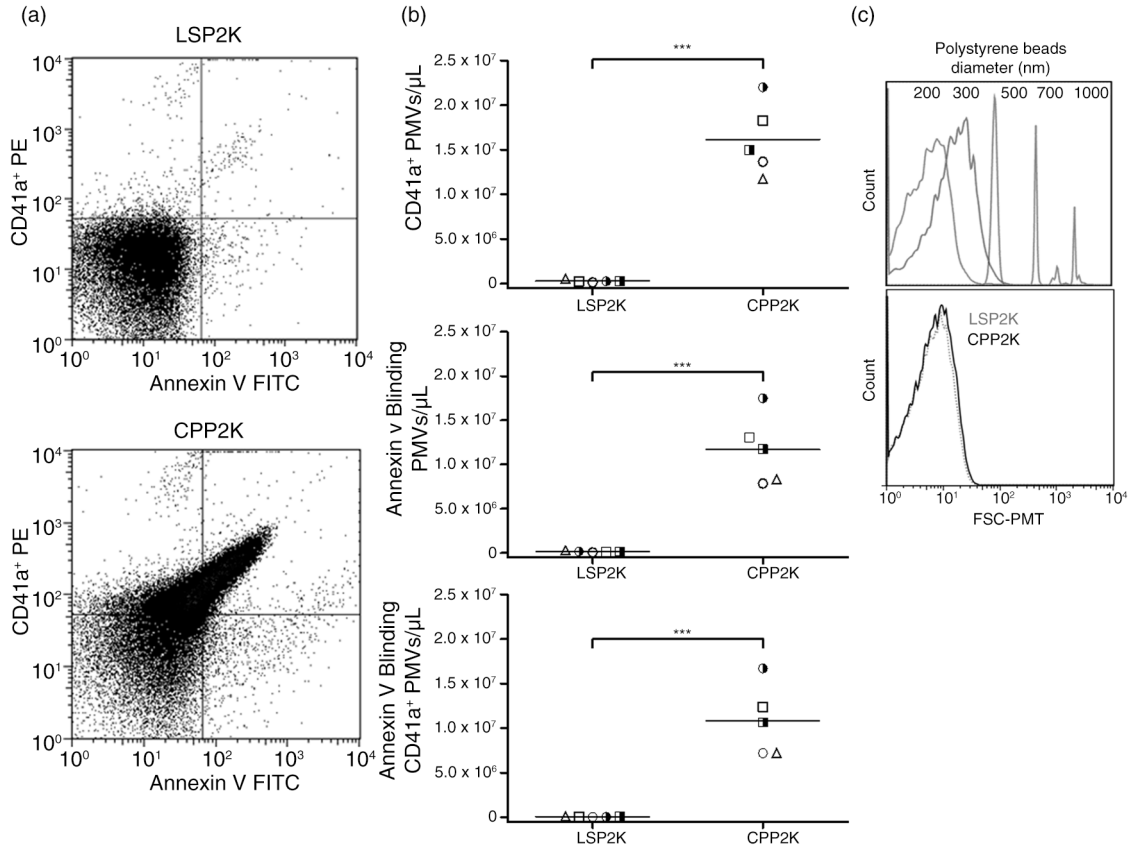

Fig. 5. Flow cytometric analysis revealed marked increase of PLT-derived extracellular microvesicles (PMVs) in cryopreserved PLTs (CPPs) compared to liquid-stored platelets (LSPs). (a) Representative annexin V (FITC)/CD41a$^+$ (PE) double fluorescence plots of PMVs in supernatants of 2,600 g spun LSPs and CPPs (LSP2K, CPP2K). (b) Counts of released annexin V binding, CD41a$^+$ and annexin V binding/CD41a$^+$ PMVs are shown in scatter plots (mean) for individual donors; n = 4; ***p < 0.001. (c) Forward scatter (FSC-PMT) histogram comparing size of LSP2K and CPP2K PMVs with that of the polystyrene bead size standards (hydrodynamic diameter, nm).

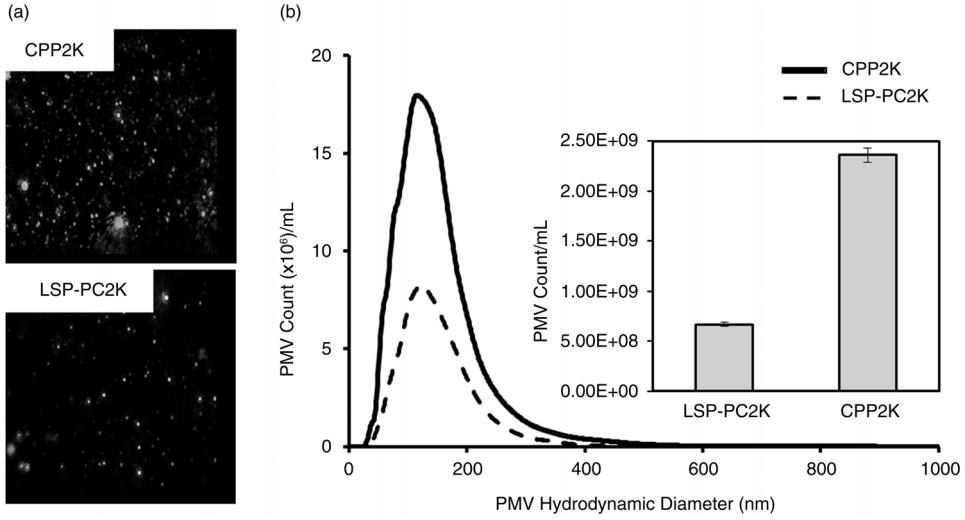

Fig. 6. Nanoparticle tracking analysis shows 5 times higher counts of exosome-size PLT-derived extracellular microvesicles (PMVs) in cryopreserved platelets (CPPs) compared with liquid-stored platelet-processing controls (LSP-PCs). (a) Representative nanoparticle tracking analysis (NTA) video frames of PLT-derived extracellular microvesicles (PMVs) in 2,600 g spun LSP-PCs and CPPs supernatants (CPP2K, LSP-PC2K). (b) Histogram showing size distribution of PMVs and bar graph showing total count of PMVs released in LSP-PC2K and CPP2K per 1 mL. Data shown in mean ± SD from n = 3 donors.

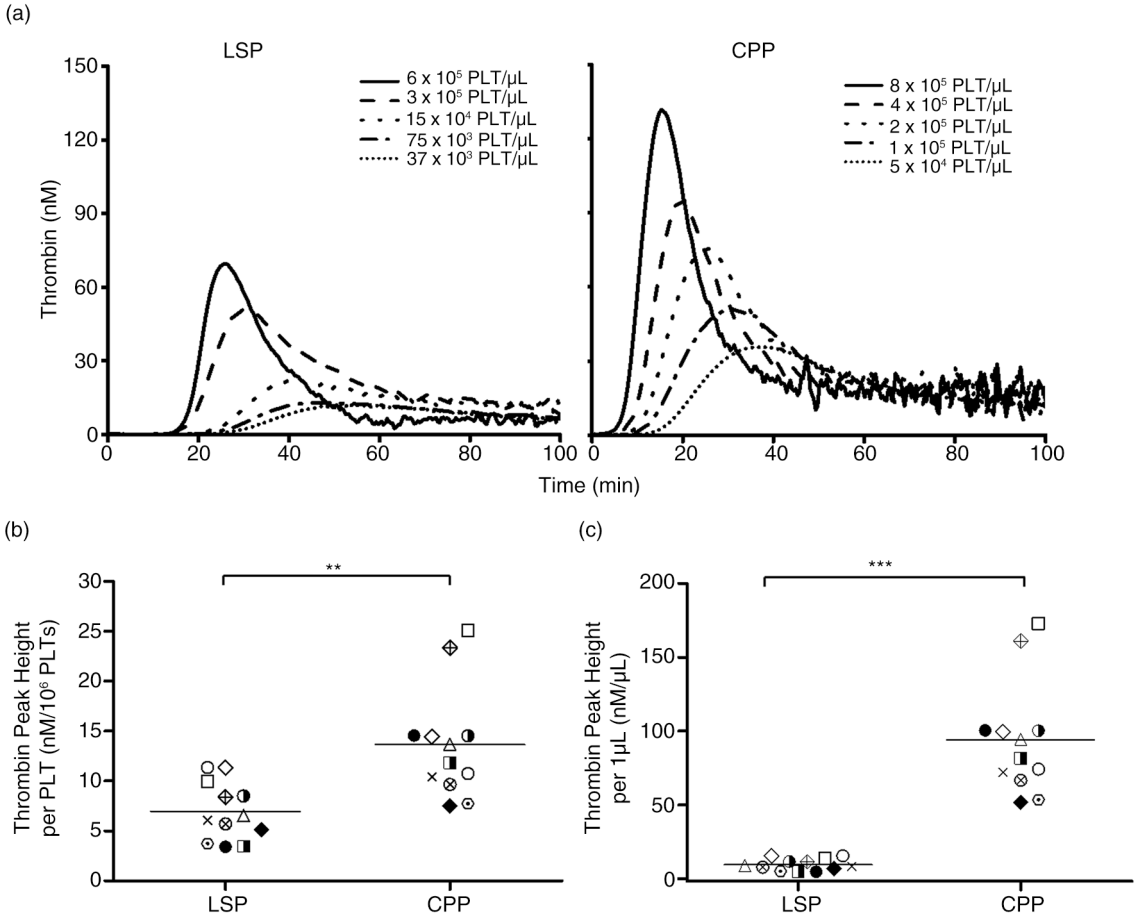

Fig. 7. Thrombin-generating procoagulant activity (TG-PCA) of cryopreserved platelets (CPPs) was 2-folds higher per PLT and 9-folds higher per µL as compared to liquid-stored platelets (LSPs). (a) Thrombin generation curve of LSPs and CPPs serially diluted in 2 folds. The first sample of LSPs, shown in solid line, was taken directly from the apheresis bag while CPPs, also shown in solid, were pre-diluted. (b) Thrombin peak height (TPH)/10^6 PLTs of LSP and CPP units. (c) TPH/1 µL of LSP and CPP units. Individual data points collected from n = 12 donors are presented in scatter plots (mean); **p < 0.01 and ***p < 0.001.

overlapping with the detection range of FC (45–47). NTA is a high-count method that can provide accurate data on the size distribution of membrane vesicles <200 nm. Whereas dynamic light scattering (DLS)-based instruments such as the Thrombolux may be useful for the detection of the presence of relative amounts of microvesicles in PLT samples (48), accurate analysis of the size distribution of PMVs is not possible using this technique because heterogeneous mixtures with a high polydispersity index yield misleading and inaccurate size distribution data in DLS (49).

A pioneering study of Johnson et al. demonstrated that CPPs express a large amount of PS and generate high numbers of PS-expressing microvesicles that contribute to the ability of CPPs to support TG in normal platelet free plasma (20). Cell membrane-exposed PS facilitates the assembly of plasma coagulation factor activating complexes, particularly FX- and prothrombin-activating complexes. We developed and applied a quantitative method for evaluation of PCA in preparations derived from stored and processed platelets. To quantify the difference in procoagulant activities, we optimized assay's analytical conditions in order to observe the dose-dependent TG activity of serially diluted LSP, CPP and PMV samples and tested them in plasma. Therefore, our assay allows determination of specific platelet potency, which is expressed as amount of thrombin generated per 1 µL of preparation or per 1 platelet. Commercial TG test is intended for evaluation of coagulation factor deficiencies and is less suitable for platelet studies. For example, commercial concentrations of synthetic lipid vesicles and relipidated tissue factor are optimized to reduce variation in PMV content in clinical samples of PPP. To investigate PS-dependent TG-PCA, the assay was performed in the presence of 0.2 pM TF, a concentration selected in preliminary experiments with PLTs and synthetic

Citation: Journal of Extracellular Vesicles 2016, 5: 30422 - http://dx.doi.org/10.3402/jev.v5.30422

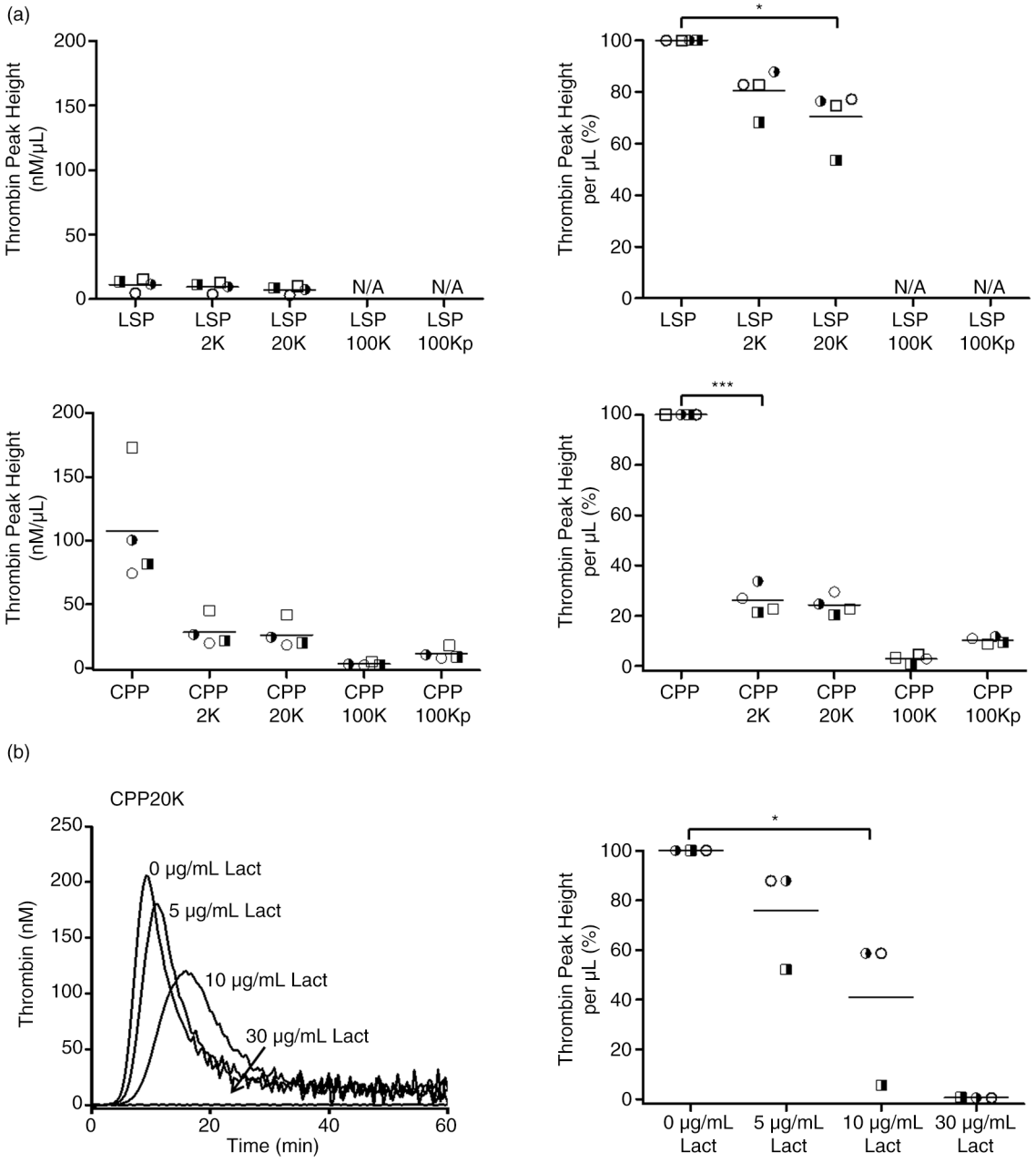

Fig. 8. Distribution of thrombin-generating procoagulant activity (TG-PCA) of liquid stored platelet (LSP) and cryopreserved platelet (CPP) products and their derived supernatants; Inhibition of TG-PCA by lactadherin. (a) TG-PCA of liquid stored platelets (LSPs) and cryopreserved platelets (CPPs) and their differentially centrifuged supernatants are presented as thrombin peak height (TPH)/µL and in % activity of corresponding LSP and CPP products. Scatter plots (mean) represent individual data points collected from n = 4 donors; *$p \leq 0.05$ and ***$p \leq 0.001$. N/A not assayed. b) Representative thrombin generation curves show the inhibition of TG-PCA of CPP20K supernatant with 5 µg/mL, 10 µg/mL and 30 µg/mL of lactadherin. Scatter plot (mean) shows individual data points as TPH/µL in % activity of CPP20K without lactadherin; n = 3 donors; *$p \leq 0.05$.

vesicle preparations. Under these conditions, robust and reproducible dose-dependent effect of LSPs and CPPs were observed in a wide range of PLT concentrations, allowing us to record TG-PCA for 120 min after recalcification. In the absence of substituted TF, even with saturation of substituted phospholipids, CPP PMVs exhibited very slow TG, with high variability. We cannot confirm a significant amount of functional contribution of TF to TG-PCA in CPPs and PMVs in CPP supernatant (20). In addition, the presence of active TF on PLTs and PMVs remains a highly controversial topic and several commercially available assays and antibodies have

been questioned with respect to the TF specificity (50). Although it remained outside the scope of our work, the data on the TF activity of CPPs and CPP PMVs (20) should be evaluated with caution.

LSP and CPP were tested at PLT concentrations relevant to respective products for clinical use (i.v. infusion). Cell counts and volumes of PLT transfusion products are donor dependent. Apheresis LSP units contain at least 3×10^{11} PLTs in 165–375 mL, resulting in a PLT concentration of about 1.5×10^{12} PLTs/L (5). In contrast, CPP unit for clinical use contain about 3×10^{11} PLTs in about 50 mL giving PLT concentration approximately 6×10^{12} PLTs/L. Haemostatic and thrombogenic potency of CPP products at the site of infusion is likely related not only to TGA/PLT but also to TGA/μL of the infused unit. The marked difference in TGA/μL between CPP and LSP warrants a caution with regard to potential adverse effects at the site of infusion.

In conclusion, our study shows for the first time that platelet membrane damage during DMSO cryopreservation is caused by membrane disintegration associated with the significant increase of membrane fluidity (membrane transition) caused by 6% DMSO alone and further aggravated by freezing–thawing process. Grape-like membrane disintegration is demonstrated by the original FESEM analysis (for the first time) and the FP data (never before applied to studies of DMSO-CPPs). Unlike previous investigations, our study includes nanoscale vesicles, thereby providing, for the first time, a comprehensive characterization of PMVs in whole size range using a panel of high-resolution techniques. These data have practical value: presented PMV size distribution, PS-dependent contribution to TG activity, and further quantitative and qualitative data are essential for product characterization supporting further clinical development of DMSO-CPP. Standardization of CPP preparation and comprehensive characterization of CPPs including relevant in vitro potency assays, such as TG-PCA, are essential for clinical studies evaluating the safety and effectiveness of CPP products.

Disclaimer

The findings and conclusions in this article have not been formally disseminated by the US Food and Drug Administration and should not be construed to represent any agency determination or policy.

Conflict of interest and funding

There are no conflicts of interests. This project was supported in part by appointments to the Research Participation Program at the Center for Biologics Evaluation and Research administered by the Oak Ridge Institute for Science and Education through an interagency agreement between the US Department of Energy and the US Food and Drug Administration.

References

1. Dumont LJ, Slichter SJ, Reade MC. Cryopreserved platelets: frozen in a logjam? Transfusion. 2014;54:1907–10.
2. Valeri CR. Hemostatic effectiveness of liquid-preserved and previously frozen human platelets. N Engl J Med. 1974;290: 353–8.
3. Valeri CR, Feingold H, Marchionni LD. A simple method for freezing human platelets using 6 per cent dimethylsulfoxide and storage at −80 degrees C. Blood. 1974;43:131–6.
4. Valeri CR, Ragno G, Khuri S. Freezing human platelets with 6 percent dimethyl sulfoxide with removal of the supernatant solution before freezing and storage at −80 degrees C without postthaw processing. Transfusion. 2005;45:1890–8.
5. Dumont LJ, Cancelas JA, Dumont DF, Siegel AH, Szczepiorkowski ZM, Rugg N, et al. A randomized controlled trial evaluating recovery and survival of 6% dimethyl sulfoxide-frozen autologous platelets in healthy volunteers. Transfusion. 2013;53:128–37.
6. Santos NC, Figueira-Coelho J, Martins-Silva J, Saldanha C. Multidisciplinary utilization of dimethyl sulfoxide: pharmacological, cellular, and molecular aspects. Biochem Pharmacol. 2003;65:1035–41.
7. Jacob SW, Herschler R. Pharmacology of DMSO. Cryobiology. 1986;23:14–27.
8. Fahy GM. The relevance of cryoprotectant "toxicity" to cryobiology. Cryobiology. 1986;23:1–13.
9. Oh JE, Karlmark Raja K, Shin JH, Pollak A, Hengstschläger M, Lubec G. Cytoskeleton changes following differentiation of N1E-115 neuroblastoma cell line. Amino Acids. 2006;31: 289–98.
10. Jiang G, Bi K, Tang T, Wang J, Zhang Y, Zhang W, et al. Down-regulation of TRRAP-dependent hTERT and TRRAP-independent CAD activation by Myc/Max contributes to the differentiation of HL60 cells after exposure to DMSO. Int Immunopharmacol. 2006;6:1204–13.
11. Cox MA, Kastrup J, Hrubisko M. Historical perspectives and the future of adverse reactions associated with haemopoietic stem cells cryopreserved with dimethyl sulfoxide. Cell Tissue Bank. 2012;13:203–15.
12. Hornsey VS, McMillan L, Morrison A, Drummond O, Macgregor IR, Prowse CV. Freezing of buffy coat-derived, leukoreduced platelet concentrates in 6 percent dimethyl sulfoxide. Transfusion. 2008;48:2508–14.
13. Valeri CR, Macgregor H, Ragno G. Correlation between in vitro aggregation and thromboxane A2 production in fresh, liquid-preserved, and cryopreserved human platelets: effect of agonists, pH, and plasma and saline resuspension. Transfusion. 2005;45:596–603.
14. Khuri SF, Healey N, MacGregor H, Barnard MR, Szymanski IO, Birjiniuk V, et al. Comparison of the effects of transfusions of cryopreserved and liquid-preserved platelets on hemostasis and blood loss after cardiopulmonary bypass. J Thorac Cardiovasc Surg. 1999;117:172–83;discussion 83–4.
15. Klein E, Toch R, Farber S, Freeman G, Fiorentino R. Hemostasis in thrombocytopenic bleeding following infusion of stored, frozen platelets. Blood. 1956;11:693–9.
16. Slichter SJ, Jones M, Ransom J, Gettinger I, Jones MK, Christoffel T, et al. Review of in vivo studies of dimethyl sulfoxide cryopreserved platelets. Transfus Med Rev. 2014;28: 212–25.
17. Schiffer CA, Aisner J, Wiernik PH. Clinical experience with transfusion of cryopreserved platelets. Br J Haematol. 1976;34: 377–85.

18. Lelkens CC, Koning JG, de Kort B, Floot IB, Noorman F. Experiences with frozen blood products in the Netherlands military. Transfus Apher Sci. 2006;34:289–98.
19. Neuhaus SJ, Wishaw K, Lelkens C. Australian experience with frozen blood products on military operations. Med J Aust. 2010;192:203–5.
20. Johnson L, Coorey CP, Marks DC. The hemostatic activity of cryopreserved platelets is mediated by phosphatidylserine-expressing platelets and platelet microparticles. Transfusion. 2014;54:1917–26.
21. Shibeko AM, Woodle SA, Lee TK, Ovanesov MV. Unifying the mechanism of recombinant FVIIa action: dose dependence is regulated differently by tissue factor and phospholipids. Blood. 2012;120:891–9.
22. Woodle SA, Shibeko AM, Lee TK, Ovanesov MV. Determining the impact of instrument variation and automated software algorithms on the TGT in hemophilia and normalized plasma. Thromb Res. 2013;132:374–80.
23. Simak J, Holada K, Janota J, Stranák Z. Surface expression of major membrane glycoproteins on resting and TRAP-activated neonatal platelets. Pediatr Res. 1999;46:445–9.
24. Simak J, Gelderman MP. Cell membrane microparticles in blood and blood products: potentially pathogenic agents and diagnostic markers. Transfus Med Rev. 2006;20:1–26.
25. Orecna M, De Paoli SH, Janouskova O, Tegegn TZ, Filipova M, Bonevich JE. Toxicity of carboxylated carbon nanotubes in endothelial cells is attenuated by stimulation of the autophagic flux with the release of nanomaterial in autophagic vesicles. Nanomedicine. 2014;10:939–48.
26. Semberova J, De Paoli Lacerda SH, Simakova O, Holada K, Gelderman MP, Simak J. Carbon nanotubes activate blood platelets by inducing extracellular Ca2+ influx sensitive to calcium entry inhibitors. Nano Lett. 2009;9:3312–7.
27. Lacerda SH, Semberova J, Holada K, Simakova O, Hudson SD, Simak J. Carbon nanotubes activate store-operated calcium entry in human blood platelets. ACS Nano. 2011;5: 5808–13.
28. Dobrovolskaia MA, Patri AK, Simak J, Hall JB, Semberova J, De Paoli Lacerda SH, et al. Nanoparticle size and surface charge determine effects of PAMAM dendrimers on human platelets in vitro. Mol Pharm. 2012;9:382–93.
29. De Paoli SH, Diduch LL, Tegegn TZ, Orecna M, Strader MB, Karnaukhova E, et al. The effect of protein corona composition on the interaction of carbon nanotubes with human blood platelets. Biomaterials. 2014;35:6182–94.
30. Shinitzky M, Barenholz Y. Fluidity parameters of lipid regions determined by fluorescence polarization. Biochim Biophys Acta. 1978;515:367–94.
31. Rooney TA, Hager R, Stubbs CD, Thomas AP. Halothane regulates G-protein-dependent phospholipase C activity in turkey erythrocyte membranes. J Biol Chem. 1993;268:15550–6.
32. Popov VM, Vladareanu AM, Bumbea H, Kovacs E, Moisescu MG, Onisai M, et al. Assessment of changes in membrane properties of platelets from patients with chronic myeloid leukaemia in different stages of the disease. Blood Coagul Fibrinolysis. 2014;25:142–50.
33. Watala C, Golanski J, Boncler MA, Pietrucha T, Gwozdzinski K. Membrane lipid fluidity of blood platelets: a common denominator that underlies the opposing actions of various agents that affect platelet activation in whole blood. Platelets. 1998;9:315–27.
34. Spector JI, Flor WJ, Valeri CR. Ultrastructural alterations and phagocytic function of cryopreserved platelets. Transfusion. 1979;19:307–12.
35. Spector JI, Skrabut EM, Valeri CR. Oxygen consumption, platelet aggregation and release reactions in platelets freeze-preserved with dimethylsulfoxide. Transfusion. 1977;17:99–109.
36. Odink J, Brank A., Platelet preservation V. Survival, serotonin uptake velocity, and response to hypotonic stress of fresh and cryopreserved human platelets. Transfusion. 1977;17:203–9.
37. Holtz GC, Davis RB. Inhibition of human platelet aggregation by dimethylsulfoxide, dimethylacetamide, and sodium glycerophosphate. Proc Soc Exp Biol Med. 1972;141:244–8.
38. Kim BK, Baldini MG. Biochemistry, function, and hemostatic effectiveness of frozen human platelets. Proc Soc Exp Biol Med. 1974;145:830–5.
39. Owens M, Cimino C, Donnelly J. Cryopreserved platelets have decreased adhesive capacity. Transfusion. 1991;31:160–3.
40. Crowley JP, Rene A, Valeri CR. Changes in platelet shape and structure after freeze preservation. Blood. 1974;44:599–603.
41. Baythoon H, Tuddenham EG, Hutton RA. Morphological and functional disturbances of platelets induced by cryopreservation. J Clin Pathol. 1982;35:870–4.
42. Murphy S, Sayar SN, Abdou NL, Gardner FH. Platelet preservation by freezing. Use of dimethylsulfoxide as cryoprotective agent. Transfusion. 1974;14:139–44.
43. Valeri CR. Cryopreservation of human platelets and bone marrow and peripheral blood totipotential mononuclear stem cells. Ann N Y Acad Sci. 1985;459:353–66.
44. van der Pol E, Coumans F, Varga Z, Krumrey M, Nieuwland R. Innovation in detection of microparticles and exosomes. J Thromb Haemost. 2013;11(Suppl 1):36–45.
45. Dragovic RA, Collett GP, Hole P, Ferguson DJ, Redman CW, Sargent IL, et al. Isolation of syncytiotrophoblast microvesicles and exosomes and their characterisation by multicolour flow cytometry and fluorescence Nanoparticle Tracking Analysis. Methods. 2015;87:64–74.
46. Dragovic RA, Southcombe JH, Tannetta DS, Redman CW, Sargent IL. Multicolor flow cytometry and nanoparticle tracking analysis of extracellular vesicles in the plasma of normal pregnant and pre-eclamptic women. Biol Reprod. 2013;89:151.
47. Gardiner C, Ferreira YJ, Dragovic RA, Redman CW, Sargent IL. Extracellular vesicle sizing and enumeration by nanoparticle tracking analysis. J Extracell Vesicles. 2013;2:19671, doi: http://dx.doi.org/10.3402/jev.v2i0.19671
48. Raynel S, Padula MP, Marks DC, Johnson L. Cryopreservation alters the membrane and cytoskeletal protein profile of platelet microparticles. Transfusion. 2015;55:2422–32.
49. Filella M, Zhang J, Newman ME, Buffle J. Analytical applications of photon correlation spectroscopy for size distribution measurements of natural colloidal suspensions: capabilities and limitations. Colloids Surfaces A. 1997;120:27–46.
50. Gardiner C, Harrison P, Belting M, Böing A, Campello E, Carter BS, et al. Extracellular vesicles, tissue factor, cancer and thrombosis – discussion themes of the ISEV 2014 Educational Day. J Extracell Vesicles. 2015;4:26901, doi: http://dx.doi.org/10.3402/jev.v4.26901